Journal of
Applied Crystallography
ISSN 0021-8898

Received 16 August 2006
Accepted 23 January 2007

Contrast variation in X-ray and neutron scattering

Heinrich B. Stuhrmann

Institut de Biologie Structurale Jean-Pierre Ebel, CEA/CNRS/UJF, F-38027 Grenoble, France, and GKSS Forschungszentrum, Geesthacht, Germany. Correspondence e-mail: stuhrmann@ibs.fr

This contribution is meant to highlight some progress in those areas of contrast variation which are known to be technically more difficult but which promise interesting applications. These concern the use of the anomalous dispersion of light elements, like sulfur and phosphorus in structural studies and experiments of polarized neutron scattering from nuclear spin polarized samples.

1. Introduction

'Suppose a region [= volume] v of constant shape to be occupied by the molecule which for the present purposes is defined as the region into which salt does not penetrate when a salt solution is substituted for water. It is assumed that the density of the liquid outside v is uniform. The effect on the value of F [= structure factor] of increasing density everywhere outside v is equivalent to that of decreasing density by an equal amount everywhere inside v, since a uniform distribution of density has no effect on F. It follows that the values F(water) − F(salt) are the F values for a region v of uniform density equal to the difference between the electron concentration of the salt solution and water'.

This argument was introduced by Bragg & Perutz (1952) to explain reversible changes in the intensities of low-order X-ray reflections from a hemoglobin crystal and to deduce from these the shape and orientation of the hemoglobin molecule occupying the volume v within the unit cell. It also the description of what became later known as contrast variation in small-angle scattering from macromolecules in solution (Stuhrmann & Kirste, 1965).

Contrast variation by solvent exchange is a low-resolution method. It is for this reason it was been abandoned in protein crystallography a few years after its introduction in 1952. In fact, the introduction of small-sized labels – one (or very few) heavy metal atoms per protein molecule – led to be the first determination of a protein structure at nearly atomic resolution (Kendrew *et al.*, 1960). About ten years later, a similar development started in small-angle scattering with the introduction of specifically deuterated macromolecules in neutron small-angle scattering (Engelman & Moore, 1972).

Somewhat earlier, in the late sixties, discussions went on about the visualization of single polymer chains in the bulk by deuteration using neutron scattering. For this purpose dilute solid solutions of the ordinary polymer in the perdeuterated polymer had to be prepared (Kirste, 1970). The study on vitreous polymethylmethacrylate showed that the unperturbed random coil is the conformation of chain molecules in the amorphous solid state (Kirste *et al.*, 1972). A number of similar studies have been published since then. A first collection of these was presented at the Third International Conference on X-ray and neutron small-angle scattering in 1973.

While the above mentioned methods are still used, new methods of contrast variation in both X-ray and neutron scattering have come up in the last twenty years. This paper will focus on anomalous or resonant contrast and nuclear spin contrast.

2. Anomalous or resonant contrast

Anomalous dispersion of X-ray optical properties accompanies the resonant absorption of energy in the transition from a bound atomic orbital to an electronic state in the continuum. This process leads to an anomalous scattering which adds to the wavelength independent atomic scattering factor f_0.

$$f = f_0 + f' + if'' \tag{1}$$

where f' and f'' are the real and imaginary components of the wavelength dependent anomalous scattering. Anomalous dispersion is strongest near X-ray absorption edges. Fig. 1 shows the resonant scattering factors of phosphates in purple membrane. The imaginary part f'' is related to the total photoelectric absorption cross section σ by the optical theorem.

$$\sigma = 2\lambda f'' b_e \tag{2}$$

with $b_e = 0.28 \times 10^{-12}$ cm, and the wavelength λ. The real component of resonant scattering, f' with its −20 eu (electron units) slightly more than compensates the non-resonant f_0 = 15 eu (electron units) (Fig. 1).

Phosphates and also sulfates develop a strong anomalous (or resonant) contrast at wavelengths near their K-absorption edges.

The anomalous dispersion of the scattering intensity is given by

$$I(Q) = \langle |U(\mathbf{Q})|^2 + 2f' \mathrm{Re}\{U(\mathbf{Q})V^{\star}(\mathbf{Q})\} + (f'^2 + f''^2)|V(\mathbf{Q})|^2 \rangle \tag{3}$$

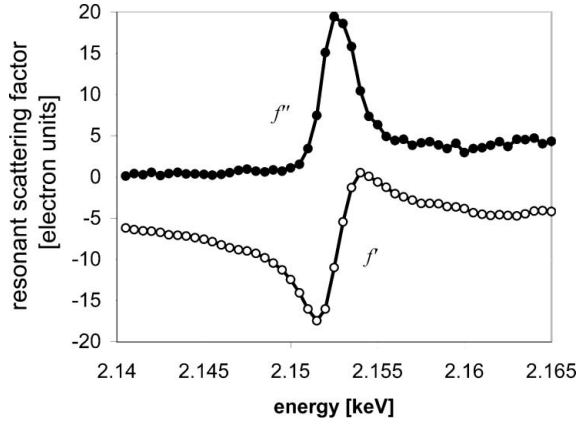

Figure 1
Resonant scattering factors of phosphate in purple membrane (Biou *et al.*, 2005).

where **Q** is the scattering vector, $Q = |\mathbf{Q}| = (4\pi/\lambda)\sin\theta$ (2θ = scattering angle), $U(\mathbf{Q})$ is the amplitude of non-resonant atoms and $V(\mathbf{Q})$ = amplitude of resonant atoms.

The average over all orientations of the macromolecule in solution denoted by $\langle ... \rangle$ starts from a development of the amplitude as a series of spherical harmonics (Stuhrmann, 1970).

Once the imaginary component $f''(\lambda)$ has been obtained from $\sigma(\lambda)$ by using equation (2), the Kramers–Kronig relation provides $f'(\lambda)$. The dispersion of the resonant scattering factors is needed for the determination of the three basic scattering functions on the right side of equation (3) from measurements of the scattering intensity at three (or more) conveniently chosen wavelengths.

Experiments of anomalous contrast variation are most conveniently performed at synchrotron radiation facilities. Anomalous small-angle X-ray scattering (ASAXS) has become the most fashionable way of contrast variation with X-rays, which again resembles very much the situation in protein crystallography. The applications have become numerous, particularly in materials science (*e.g.* Simon, 2007; Goerigk *et al.*, 2003). The study of polyelectrolytes has become most rewarding, as ASAXS allows contrast variation at constant chemical potential. An illustrative example is a recent study of the Sr^{2+} ions around the polyacrylate chain (Goerigk *et al.*, 2004).

Light elements like phosphorus, sulfur, chlorine and calcium are wide spread, particularly in living matter. RNA, DNA and membranes contain phosphorus. Sulfur is a regular constituent of proteins. Anomalous scattering from phosphorus and sulfur is a potentially powerful tool in structural studies on nucleoproteins and membrane proteins.

Experiments of small-angle scattering from solutions are technically more difficult with soft X-rays. The penetration depth of about 1 mm of X-rays in water at λ = 1.5 Å drops to 20 µm at wavelengths near the *K*-absorption edge of phosphorus (λ_K = 5.76 Å). A liquid sample then is kept between two thin elastically stretched plastic foils kept at a distance of not more than 30 µm in an evacuated environment (Hütsch, 1992). The results of such an experiment are shown in Fig. 2.

The conditions of solution scattering at wavelengths near the *K*-edge of sulfur (λ_K = 5.018 Å, or E = 2470 keV) are slightly less stringent than with phosphorus as the penetration depth increases to 30 µm water. Anomalous scattering from sulfur has been used for the study of polymers (Mardalen *et al.*, 1994) and on various chiral smectic phases of liquid crystals (Mach *et al.*, 1998). Moreover, sulfur exhibits valence states between −2 in sulfides and +6 in sulfates, which influence the resonance energy considerably. The absorption edge of sulfates is shifted by 10 eV towards higher energies with respect to that of sulfides (Pickering *et al.*, 1998). Anomalous scattering from sulfur in the valence state −2 (*e.g.* in methionine or cysteine, regular constituents of proteins) can be measured easily even in the presence of a high sulfate concentration (Stuhrmann, 1994).

The reduced penetration depth of soft X-rays necessitates a complete redesign of all components of an X-ray synchrotron radiation beamline (Biou *et al.*, 2005; Djinović Carugo *et al.*, 2005).

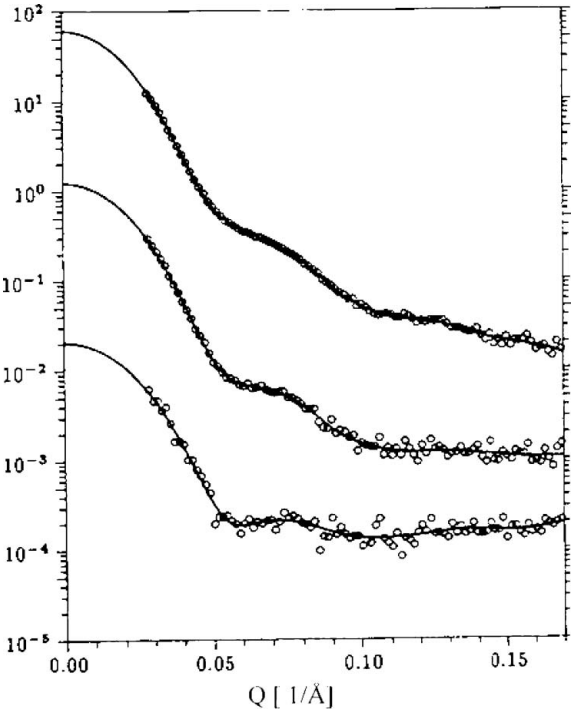

Figure 2
The basic scattering functions of the large subunit of *E. coli* ribosomes from ASAXS at wavelengths near the *K* absorption edge of phosphorus. The upper curve is $\langle |U(\mathbf{Q})|^2 \rangle$ which does not depend on the wavelength. The lowest $\langle |V(\mathbf{Q})|^2 \rangle$ is the scattering intensity of the phosphorus atoms of the ribosomal RNA. The cross term $2\langle \mathrm{Re}\{U(\mathbf{Q})V^*(\mathbf{Q})\} \rangle$ is in the middle of the figure. The open spheres are the values of the basic scattering functions deduced from seven scattering functions measured at wavelengths near the *K*-edge of phosphorus. The line is obtained from an indirect method using the anomalous dispersion of the distance distribution function. There are about 1500 P atoms per 1500 kD of the ribosomal subunit. The intensity scale is given in arbitrary units. The data were obtained at the beamline A1 of HASYLAB (Hütsch, 1992).

3. Isotopic and nuclear spin contrast

Contrast variation by isotopic substitution is widely used in neutron small-angle scattering. Hydrogen is the most important player in this game. While the scattering length of coherent scattering of its heavier isotope, ^{2}H (= D for deuterium) is similar to average of scattering lengths of other elements, ^{1}H (= H) shares its negative scattering length with very few other isotopes. In soft condensed matter research this property of ^{1}H is unique.

Both H and D have non-spinless nuclei, which are amenable to high polarization under conditions which will be described below. In polarized neutron scattering, there is a strong variation of the scattering length b of ^{1}H with proton polarization P(H) and a much weaker one for ^{2}H with deuteron polarization P(D).

$$b(\mathrm{H}) = [-0.374 \pm 1.456\mathrm{P(H)}]10^{-12}\,\mathrm{cm} \quad (4)$$

$$b(\mathrm{D}) = [+0.66 \pm 0.28\mathrm{P(D)}]10^{-12}\,\mathrm{cm} \quad (5)$$

The sign ± stands for neutron beam polarization which is assumed to have the values of either p = +1 or p = −1. The values of nuclear polarization may vary between +1 and −1. While almost completely polarized neutron beams are obtained routinely by spin filtering, the interval of nuclear polarization values will be smaller. The large variation of the scattering length with P(H) goes together with the incoherent scattering, which is strong for unpolarized protons. There is no incoherent scattering when pP = +1, *i.e.* when the direction of nuclear spin polarization and neutron spin polarization point into the same direction (Glättli & Goldman, 1987).

It must be noted that the scattering length b is a complex number (1). As absorption of the neutron by the nucleus followed by the disintegration of the latter is rare with elements of soft condensed matter, the preceding equations of X-ray scattering can be used for neutron scattering, but without the imaginary part of resonant scattering f''.

Nearly all experiments of contrast variation in neutron scattering rely on the isotopic substitution of H by D. This method has been and still is successful for two reasons: first, the difference in scattering length $b(\mathrm{H}) - b(\mathrm{D})$ is large, and second, hydrogen is by far the most abundant element in soft condensed matter. Both factors together assure a high contrast. An account on experiments of neutron scattering in H_2O/D_2O mixtures has been given by Li *et al.* (1983) and Perkins (1988).

For twenty years, ribosomes have been intensively studied using neutron scattering. Triangulation between selectively deuterated ribosomal proteins has led to their spatial arrangement in the small subunit of *E. coli* ribosomes (Ramakrishnan *et al.*, 1984).

While the determination of the co-ordinates of the 21 ribosomal proteins by specific deuteration was a major success of neutron scattering in structural biology, the application of the same method to the large subunit of the ribosome with its 34 ribosomal proteins (about 1/3 of the total weight, the rest being rRNA) turned out to be prohibitively difficult, not to mention the functional complex of the ribosome consisting of the two ribosomal subunits with tRNA and mRNA attached to it. It was this challenge which led to the more powerful method of nuclear spin contrast variation.

As stated in equation (4) the variation of the scattering length, $b(\mathrm{H})$, due to proton spin polarization, exceeds that due to isotopic exchange by a factor which may larger than 2. Moreover contrast variation by nuclear polarization would be done with the same sample. Systematic errors due to the comparison of different samples, as they are needed in contrast variation by isotopic substitution, are avoided.

Nuclear spin contrast variation is used at its best with specifically deuterated macromolecules. Thus, the nuclear polarization is used to enhance an already existing contrast. The variation of the intensity of incoherent scattering from ^{1}H was reduced by massive deuteration of the sample. The ribosome molecule was perdeuterated, the region of interest being excepted. As an example, the protein L3 of the large subunit remained protiated while the rest of the particle and the solvent were deuterated. For the study of the functional complex of the ribosome, the protiated tRNA was bound to the deuterated ribosome. A number of specifically deuterated ribosomes were studied by proton contrast variation and by deuteron contrast variation (Willumeit *et al.*, 2001; Nierhaus *et al.*, 1998; Knop *et al.*, 1992) (Fig. 3).

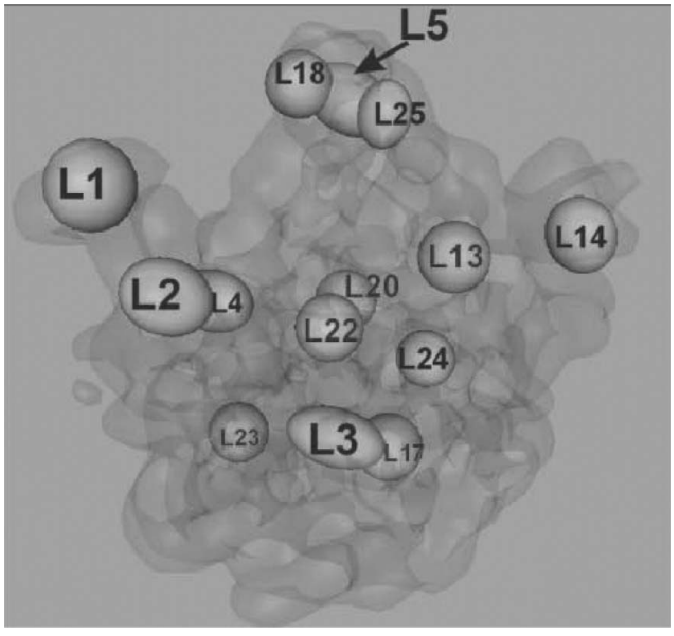

Figure 3
Positions of ribosomal proteins of the large subunit of *E. coli* ribosomes determined by nuclear spin contrast variation (Willumeit *et al.*, 2001).

Experiments of polarized neutron small-angle scattering from nuclear spin polarized samples started in the mid eighties. While at the GKSS Research Centre, Geesthacht, Germany, biological structures were preferred (Knop, 1986), Glättli and coworkers at CEA, Saclay France, started a program of proton spin contrast variation on polymers (Glättli, 1989) and so did Kohgi and his co-workers at KEK, Japan, who started with crown ether solutions (Kohgi *et al.*, 1987; Masuda *et al.*, 1988).

4. Dynamic nuclear spin contrast

All experiments mentioned above used the method of dynamic nuclear polarization (DNP). All samples contained a small number of paramagnetic centers which in a microwave field 'catalyse' nuclear polarization. A high nuclear polarization by DNP can be obtained in a magnetic field $B \geq 2$ T at temperatures ≤ 1 K. The direction of nuclear polarization with respect to the external field can be positive or negative depending on the choice of the microwave frequency. The method of DNP is an extremely versatile tool of nuclear polarization (Abragam & Goldman, 1978, 1982; Glättli & Goldman, 1987).

In a simple microscopic picture of DNP, the nuclear polarization develops near paramagnetic centers through the electron–nuclear dipolar interaction decreasing with the third power of the distance between electron and nuclear moments. More distant bulk protons are polarized by dipolar interactions between nuclei (spin diffusion). The same mechanism in the reverse order is responsible for nuclear relaxation in most insulating solids.

This picture allows for the assumption that a nuclear polarization gradient should exist near paramagnetic centers. Although not easily detected at high nuclear polarization (Kohgi *et al.*, 1987), it might appear more clearly at the onset of microwave irradiation. The periodic change of the direction of the polarization by changing the microwave frequency greatly facilitated the experiment of time-resolved polarized neutron scattering (van den Brandt *et al.*, 2002).

The results obtained from time-resolved neutron scattering and simultaneous NMR measurements with sodium bis(2-hydroxy-2-ethylbutyrato)oxochromate, $C_{12}H_{20}CrO_7Na$ [abbreviated as EHBA-Cr(V)], in glycerol–water mixtures with different degrees of deuteration suggest that a high polarization of the 20 protons of the EHBA-Cr(V) complex develops within a second and that the polarization of the residual protons of the deuterated solvent increases at a much lower rate.

At this point one might argue that the concentration gradient of protons at the surface of the dissolved radicals could be responsible for the delayed polarization of the bulk protons in the solvent. Experiments with samples of lower deuteration of the solvent showed that the initial built-up of the local polarization did not decrease as much as expected (van den Brandt *et al.*, 2003, 2006). It must be assumed that the proton concentration gradient is not the only reason for the relative leak tightness of the polarized proton domain. In fact a small shift of the Larmor frequency of the close protons due to the local magnetic field might reduce their contact with the bulk protons of the solvent (Hayter *et al.*, 1974).

With radicals of bigger size the polarization gradient might lie inside the radical molecule. Promising candidates were DPPH [2,2′-di(4-*tert*-octylphenyl)-1-picryl-hydrazyl] and a biradical with an inter-radical distance of 38 Å, both embedded in a matrix of perdeuterated

polystyrene and both of which support DNP efficiently. From a preliminary analysis of neutron scattering from the biradical it appears that the polarization gradient extends to about 10 Å from each of the radical sites and that there is free spin diffusion beyond this distance (Stuhrmann, 2007).

The measurement of the speed of free nuclear spin diffusion requires much bigger particles. An elegant approach to this problem comes from J. Kohlbrecher, who suggested polystyrene spheres (800 Å diameter) embedded in a glycerol–water mixture rich in EHBA-Cr(V). Time-resolved polarized neutron scattering did reveal changes of the apparent radius of gyration which can be assigned unambiguously to the penetration of polarization into the nanospheres (van den Brandt *et al*, 2007).

Knowing the size of proton spin domains and their life-time is essential for the analysis of dynamic nuclear spin contrast from more complex structures like catalase. Its paramagnetic center, a tyrosine radical that develops on addition of peroxyacetic acid, supports DNP like the previously mentioned radicals. The important difference with respect to the experiments discussed above is the concentration of paramagnetic centers which are about 200 times lower. The time-dependent neutron scattering intensity drops by the same factor. The same is true for the measurement of time dependent NMR. The scattering amplitude of the protons close to the unpaired electron of the tyrosine radical has been found to be 16 times larger than the amplitude of magnetic scattering. The tyrosine transformed into a radical appears to be relatively close to the heme group (Stuhrmann, 2004).

5. Electron-proton spin interaction

The probability W of dynamic nuclear polarization by the solid effect (Abragam & Goldman, 1982) is

$$W_{\text{solid effect}}(\mathbf{r}) \sim (\sin\vartheta\cos\vartheta/r^3)^2 \qquad (6)$$

r and ϑ are polar co-ordinates. The direction of the magnetic field is along $\vartheta = 0$.

From equation (6) it appears that those EHBA-Cr(V) molecules that happen to have the direction of their long axis at an angle close to $\vartheta = 45°$ with respect to the external magnetic field are more susceptible to DNP (Fig. 4). The dumb-bell like repartition of the hydrogen atoms to some extent stabilizes the preferential proton

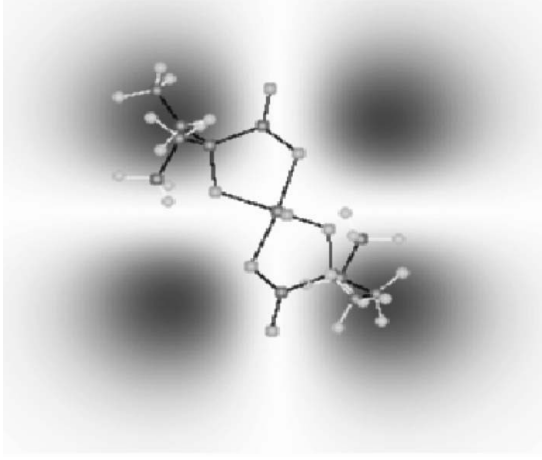

Figure 4
The EHBA-Cr(V) molecule in an orientation that is favorable for DNP.

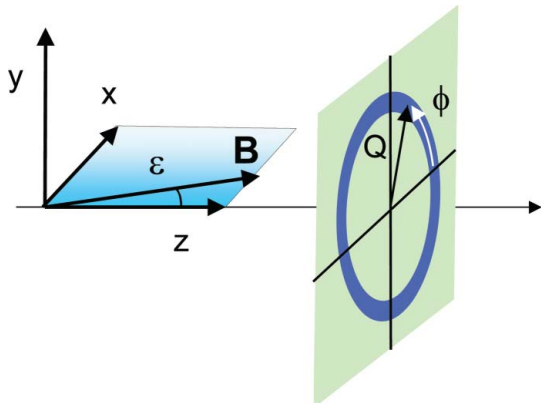

Figure 5
The scattering geometry. The direction of the neutron beam coincides with z. The direction of the magnetic field **B** in the (x,z) plane differs from that of the neutron beam by the angle ε (left side of the figure). The detector plane with Q and the azimuth angle ϕ is shown on the right side.

polarization in each of the two groups of 10 H atoms (Fig. 4). Typically 2 to 3 out of the 10 protons will get polarized during the built-up of local polarization. An asymmetric distribution of the intensity of small-angle scattering will result, even if there is a rapid exchange of spin states within each group of 10 protons of the EHBA-Cr(V) molecule. The asymmetry depends on the angle ε between the direction of the magnetic field and the direction of the neutron beam (Fig. 5).

There is no asymmetry of the intensity distribution if the direction of the neutron beam coincides with the direction of the magnetic field. For finite angles between the neutron beam and the magnetic field direction, one clearly distinguishes the contribution from the spherical harmonics Y_{lm} with $l = 2$ and $l = 4$ (Fig. 6).

In the absence of spin state exchange between the nuclei close to the paramagnetic center, the asymmetry would increase by a factor 2 at $Q = 0.3$ Å^{-1} and up to a factor 5 for $Q = 0.85$ Å^{-1}. Polarized neutron scattering could show on the way to how close proton spins interact with each other, how they are influenced by the polarized electron spin, and how their polarization propagates into the bulk.

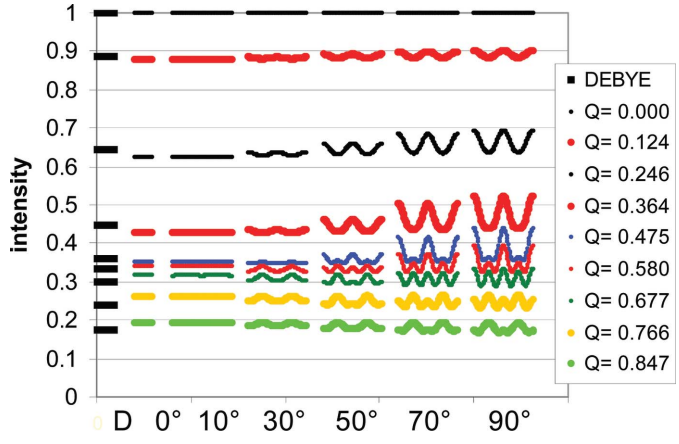

Figure 6
The variation of the time-dependent intensity of small-angle scattering from EHBA-Cr(V) in a deuterated solvent with the azimuth angle ϕ (0° to 360°) on the area detector at different Q [1 Å^{-1}] (from $Q = 0$ at the top and $Q = 0.847$ Å^{-1} at the bottom) and at different angles between the direction of the external magnetic field and the direction of the neutron beam (0°, 10°, 30°, 50°, 70°, 90°). The scattering intensity in the absence of orientation dependent DNP is denoted by D (Debye equation of solution scattering). The corresponding intensity of incoherent scattering is comparable with that of coherent zero-angle scattering.

Most of our time-resolved experiments of neutron scattering from dynamically polarized proton spins have been done with a magnetic field direction off-set angle of 7° with respect to the neutron beam. This angle, at that time, had been chosen in order to cover larger angles on the detector in the asymmetric position at D22 of the ILL. Small though the off-set angle is, it is presently attempting to extract the predicted asymmetry from an average of all the time-resolved neutron scattering data collected from EHBA-Cr(V) so far. Needless to say, that an increase of the off-set angle to 30° – this is possible with the polarization facility of the PSI – would increase the asymmetry of intensity exclusively due to electron spin–proton spin interaction by almost two orders of magnitude.

6. Outlook for the future

In X-ray small-angle scattering, anomalous contrast variation has reached a high technical reliability at various synchrotron radiation facilities. The extraction of the purely resonant term from a set of data measured at more than two wavelengths near an absorption edge is an important progress, as it gives direct access to the spatial correlation between resonant atoms in very complex materials. As this term comes along as a small difference between large intensities, its determination is becoming easier at the more powerful synchrotron radiation sources of the third generation. The use of native resonant atoms in biological macromolecules, like sulfur and phosphorus, is still a technical challenge. In general, radiation damage needs to controlled carefully, as it concerns primarily the resonant atom.

In neutron scattering, there is no significant radiation damage with soft condensed matter. In some cases, this may be a reason to prefer neutrons instead of X-rays. Neutron scattering offers ideal conditions for contrast variation by substitution of the hydrogen isotope ^{1}H by ^{2}H, a technique of continuing interest. Using polarized neutrons, proton spin polarization opens a new dimension to contrast variation, that is both more powerful than deuteration and quite versatile in its applications. The latter point alludes to the properties of dynamic nuclear spin polarization and hence to the strong link with NMR and EPR methods (Buckingham, 2003; Hu *et al.*, 2004). Although time-resolved polarized neutron scattering focusing at the onset of proton polarization has revealed the time-scale of local polarization build-up near paramagnetic centers, the size and shape of polarized proton spin domains need to be studied in more detail. So far it appears that the amplitude owing to polarized proton spins near paramagnetic centers develops in less than one second and that it exceeds that of magnetic scattering due to an unpaired electron by an order of magnitude. Dynamic proton spin contrast variation is applicable to the study of dilute paramagnets, *e.g.* radicals in proteins.

The construction and implementation of nuclear polarization facilities at thermal neutron beam facilities will require an interdisciplinary collaboration where neutron physicists, particle/nuclear physicists and others are involved.

The more recent experiments of time-resolved polarized neutron scattering were done at the Institut Laue-Langevin (ILL), Grenoble, the Laboratoire Léon Brillouin, Saclay, and at the Paul-Scherrer Institute (PSI), Villigen. The facility for DNP has been built at the PSI and it has been used at the ILL on several occasions. The progress of soft X-ray scattering is the result of a collaboration with the European Molecular Biology Laboratory (EMBL) and the European Synchrotron radiation facility (ESRF).

References

Abragam, A. & Goldman, M. (1978). *Rep. Prog. Phys.* **41**, 395–467.
Abragam, A. & Goldman, M. (1982). *Nuclear Magnetism: Order and Disorder*. Oxford: Clarendon Press.
Biou, V., Bösecke, P., Bois, J.-M., Brandolin, G., Kahn, R., Mas, C., Nauton, L., Nury, H., Pebay-Peyroula, E., Vicat, J. & Stuhrmann, H. (2005). *J. Synchrotron Rad.* **12**, 402–409.
Bragg, W. L. & Perutz, M. F. (1952). *Proc. Royal Soc.* A**213**, 425–435.
Brandt, B. van den, Glättli, H., Grillo, I., Hautle, P., Jouve, H., Kohlbrecher, J., Konter, J. A., Leymarie, E., Mango, S., May, R. P., Michels, A., Stuhrmann, H. B. & Zimmer, O. (2006). *Eur. Phys. J.* B**49**, 157–165.
Brandt, B. van den, Glättli, H., Grillo, I., Hautle, P., Jouve, H., Kohlbrecher, J., Konter, J. A., Leymarie, E., Mango, S., May, R. P., Stuhrmann, H. B. & Zimmer, O. (2002). *Europhys. Lett.* **59**, 62–67.
Brandt, B. van den, Glättli, H., Grillo, I., Hautle, P., Jouve, H., Kohlbrecher, J., Konter, J. A., Leymarie, E., Mango, S., May, R. P., Stuhrmann, H. B. & Zimmer, O. (2003). *Phys. B*, **335**, 193–195.
Brandt, B. van den, Glättli, H., Hautle, P., Kohlbrecher, J., Konter, J. A., Michels, A., Stuhrmann, H. B. & Zimmer, O. (2007). *J. Appl. Cryst.* **40**, s106–s110
Buckingham, A. D. (2003). *Chem. Phys. Lett.* **371**, 517–521.
Djinović Carugo, K., Helliwell, J. R., Stuhrmann, H. & Weiss, M. S. (2005). *J. Synchrotron Rad.* **12**, 410–419.
Engelman D. M. & Moore, P. B. (1972). *Proc. Natl Acad. Sci. USA*, **69**, 1997.
Glättli, H., Fermon, C. & Eisenkremer, M. (1989). *J. Phys.* **50**, 2375–2388.
Glättli, H. & Goldman, M. (1987). *Methods Exp. Phys.* **23**C, 241–286.
Goerigk, G., Haubold, H. G., Lyon, O. & Simon, J. P. (2003). *J. Appl. Cryst.* **36**, 425–429.
Goerigk, G., Schweins, R., Huber, K. & Ballauf, M. (2004). *Europhys. Lett.* **66**, 331–337.
Hayter, J. B., Jenkin, G. T. & White, J. W. (1974) *Phys. Rev. Lett.* **33**, 696–699.
Hu, K.-N., Yu, H., Swager, T. M. & Griffin, R. G. (2004). *J. Am. Soc.* **126**, 10844–10845.
Hütsch, M. (1992). Thesis, University of Hamburg, Germany.
Kendrew, J. C., Dickerson, R. E., Strandberg, B. E., Hart, R. G., Davies, D. R., Phillips, D. C. & Shore, V. C. (1960). *Nature* (*London*), **185**, 422–427.
Kirste, R. G. (1970). Jahresber. 1969 des Sonderforschungsbereichs 41, Mainz, p. 47.
Kirste, R. G., Kruse, W. & Schelten, J. (1972). *Makromol. Chem.* **162**, 299–303.
Knop, W., Nierhaus, K. H., Novotny, V., Niinikoski, O., Krumpolc, M., Rieubland, J.-M., Rijllart, A., Schärpf, O., Schink, H. J., Stuhrmann, H. B. & Wagner, R. (1986). *Helv. Phys. Acta*, **50**, 741–746.
Knop, W., Hirai, M., Schink, H.-J., Stuhrmann, H. B., Wagner, R., Zhao, J., Schärpf, O., Crichton, R. R., Krumpolc, M., Nierhaus, K. H., Niinikoski, T. O. & Rijllart, A. (1992). *J. Appl. Cryst.* **25**, 155–165.
Kohgi, M., Ishida, M., Ishikawa, Y., Ishimoto, S., Kanno, Y., Masaike, A., Masuda, Y. & Morimoto, K. (1987). *J. Phys. Soc. Jpn*, **56**, 2681–2688.
Li, Z. Q., Perkins, S. J. & Loucheux-Lefebre, M. H. (1983). *Eur. J. Biochem.* **130**, 275–279.
Mach, P., Pindak, R., Levelut, A. M., Barois, P., Nguyen, H. T., Huang, C. C. & Furenlid, L. (1998). *Phys. Rev. Lett.* **81**, 1015–1018.
Mardalen, J., Riekel, C. & Müller, H. (1994). *J. Appl. Cryst.* **27**, 192–195.
Masuda, Y., Ishimoto, S., Ishida, M., Ishikawa, Y., Kohgi, M. & Masaike, A. (1988). *Nucl. Instrum. Methods Phys. Res. A*, **264**, 169–172.
Nierhaus, K.H. Wadzack, J., Burkhardt, N., Jünemann, R., Meerwinck, W., Willumeit, R. & Stuhrmann, H. B. (1998). *Proc. Natl Acad. Sci. USA*, **95**, 945–950.
Perkins, S. J. (1988). *Biochem. J.* **254**, 313–327.
Pickering, I. J., Prince, R. C., Drivers, T. & George, G. N. (1998). *FEBS Lett.* **441**, 11–14.
Ramakrishnan, V., Capel, M., Kjeldgaard, M., Engelman, D. M. & Moore, P. B. (1984). *J. Mol. Biol.* **174**, 265–284.
Simon, J.-P. (2007). *J. Appl. Cryst.* **40**, s1–s9.
Stuhrmann, H. B. (1970). *Acta Cryst.* A**26**, 297–306.
Stuhrmann, H. B. (1994). *Synchrotron Radiation in Biosciences*, pp. 119–138, Oxford: Clarendon Press.
Stuhrmann, H. B. (2007). *J. Phys. IV France*. In the press.
Stuhrmann, H. B. (2004). *Rep. Prog. Phys.* **67**, 1073–1115.
Stuhrmann, H. B. & Kirste, R. (1965). *Z. Phys. Chem. (Frankfurt am Main)*, **46**, 247–250.
Willumeit, R., Diedrich, G., Forthmann, S., Beckmann, J., Stuhrmann, H. B. & Nierhaus, K.H. (2001). *Biochim. Biophys. Acta*, **1520**, 7–20.